# CrystEngComm

Accepted Manuscript

This article can be cited before page numbers have been issued, to do this please use: Y. XIE, S. K. Verma, R. Verma, D. Xiong, W. Chen, C. Hu, T. A. Emmanuel, M. Wang and X. Zhao, *CrystEngComm*, 2017, DOI: 10.1039/C7CE00223H.




ROYAL SOCIETY OF CHEMISTRY

rsc.li/crystengcomm

View Article Online
DOI: 10.1039/C7CE00223H

Journal Name

ARTICLE

Received 00th January 2017,

Accepted 00th January 20xx

DOI: 10.1039/x0xx00000x

www.rsc.org/

# Heat-up and gram-scale synthesis of Cu-poor CZTS nanocrystals with controllable compositions and shapes

Santosh Kumar Verma[a,b], Rameshwari Verma[a], Yi Xie*[a], Dehua Xiong[a], Wenhui Chen[a], Chao Hu[a], Tsiwah Acheampong Emmanuel[a], Mingqing Wang[c], Xiujian Zhao*[a,b]

We report the gram-scale synthesis of Cu-poor CZTS nanocrystals (NCs) with tuned shape and composition, by using a facile phosphine-free heat-up procedure. Based on the detailed characterization and analyses on the evolution of crystal phases, composition, morphologies and optical spectra over the reaction stage and temperature, we explore the reaction mechanism. The synthesis reaction involves the formation of binary CuS (covellite) nanoparticles at room temperature, and the conversion from the as-formed CuS to intermediated Zn-Sn-codoped CuS NCs at 150 ºC and finally to quaternary CZTS NCs in kesterite phase at 220 ºC, during which the NCs gradually grow due to the progressive incorporation of foreign cations ($Zn^{2+}$ and $Sn^{2+}$) to the as-formed CuS NCs. The introduction of dodecanethiol (DT) leads to the formation of bullet-like CZTS NCs in wurtzite phase. The Cu-poor CZTS synthesis is reproducible by up-scaling the amounts of chemicals and solvent/ligand, which allows us for a promising approach of gram-scale production of Cu-based chalcogenides for potential applications in photovoltaics.

## Introduction

Quaternary copper-based chalcogenides, particularly $I_2$-II-IV-$VI_4$ compounds including copper zinc tin sulfide ($Cu_2ZnSnS_4$, CZTS), copper zinc tin selenide ($Cu_2ZnSnSe_4$, CZTSe) and CZTSSe have garnered considerable attention in the past years and have been extensively explored as potential applications in the fields of photovoltaics (PVs)[1-5] and thermoelectric materials.[6-8] Among these compounds CZTS emerged as a promising photovoltaic (PV) material due to many advantages such as earth-abundant, low-cost and relatively non-toxic component elements, optimal direct band gap (~1.5 eV) and high absorption coefficients (>$10^4$ $cm^{-1}$) in wavelength of visible region.[9-16] CZTS compound presents variety of compositions and crystallographic systems including kesterite, zincblende and wurtzite,[17-19] both are great importance to the performance of the PVs derived from the absorber layer of CZTS NPs.[14, 20] It was experimentally demonstrated that in PV devices fabricated with CZTS materials, Cu-poor (i.e. [Cu]/([Sn]+[Zn])<1) composition offered improved properties and performances. [21, 22] Consequently, a fine control of the crystal structure and cation ratios in the CZTS NCs during the synthesis is fundamental and critical to optimize functional properties.

On the other side, among various approaches of fabricating thin films for PVs, low-cost solution-based technique has emerged as compelling alternative to vacuum ones. Overall, the solution-based methods might be either a molecular precursor solution procedure followed by thermal annealing etc., [2, 10, 23-26] or a deposition of colloidal NCs which involves casting or printing the NC dispersions on various substrates.[27-29] Compared with a vacuum route, the colloidal deposition offers potential advantages such as low cost of equipment, good compatibility with flexible substrates and high throughput production.[27-29] In order to obtain colloidal CZTS NCs for PVs, various synthesis approaches including heat up,[30-35] hot injection,[36-38] hydrothermal,[39] thermolysis[40] and cation exchange[41], have been explored in the past years. Among these techniques heat-up procedure, with the advantages including scalability and well-controlled physic-chemical properties of the produced NCs, has gained popularity by many groups after Steinhagen *et al*. reported for the first time the generation of kesterite phase CZTS *via* this method. [42] In their work, CZTS NCs with average crystal size of 10.6 ± 2.9 nm were obtained by heating the suspended mixture of metal precursors (salts serving as Cu, Zn and Sn sources) and anion precursor (elemental sulfur) in oleylamine (OM) at 280 °C for 1 h.

The synthesis of quaternary NCs by either hot injection or heat up approach involves the formation of intermediated binary or ternary NCs due to the different reactivities between various cationic and anionic precursors, which is very essential for the control of the shape and composition of the resulting quaternary NCs.[43] Few reports on monitoring the evolution of Cu-poor CZTS formation are available yet although much effort has been made in tuning the morphologies and compositions of CZTS NCs. In our

[a] S State Key Laboratory of Silicate Materials for Architectures, Wuhan University of Technology, No. 122, Luoshi Road, Wuhan 430070, P. R. China. E-mail: xiey@whut.edu.cn; Tel.: +86-15527835639; E-mail: opluse@whut.edu.cn
[b] School of Civil Engineering and Architecture, Wuhan University of Technology, No. 122, Luoshi Road, Wuhan 430070, P. R. China.
[c] UCL Institute for Materials Discovery, University College of London, Room 107, Roberts Building, Malet Place, London WC1E 7JE, United Kingdom
Electronic Supplementary Information (ESI) available: [Additional TEM/HRTEM images, XRD patterns, optical spectra, TGA, determination of band gaps, size distribution histograms.]. See DOI: 10.1039/x0xx00000x

View Article Online
DOI: 10.1039/C7CE00223H




previous report on the heat-up synthesis of CIGS NCs, we observed the formation of binary covellite (CuS) during the heating process.[44] The intermediated CuS NCs acted as seeds for the following formation of CIGS due to the incorporation of $In^{3+}$ and $Ga^{3+}$ into the as-formed CuS NCs.

All the above-mentioned motivated us to investigate the crystal shape/phase control and to understand the related reaction mechanism of Cu-poor CZTS using a facile heat-up procedure. This method is phosphine-free and just involves mixing the metal precursors with S precursors, both pre-dissolved in octadecene (ODE) and OM, followed by degassing and heating up to 220 °C (as the typical reaction temperature) for 30 min. It is interesting that the synthesis involves the conversion from binary CuS at room temperature (RT) to Zn-Sn-codoped CuS NCs at 150 °C during the heating, and finally to quaternary CZTS at 220 °C. By scaling up the amount of all chemicals/solvent to 10 fold in the synthesis we could obtain gram-scale (e.g. 1.164 g) Cu-poor CZTS NCs in one-pot reaction.

## Experimental

### Materials

Analytical grade copper (II) chloride dehydrate ($CuCl_2 \cdot 2H_2O$, 98%), tin (II) chloride ($SnCl_2$, 99.99%) and sulfur metal powder (S, 99.9%) analytical grade were purchased from Sinopharm Chemical Reagent Co. Ltd., 1-octadecene (ODE, 90%), dodecanethiol (DT, 98.0%), oleylamine (OM, 70%) and zinc chloride ($ZnCl_2$, 99.99%) were purchased from Sigma Aldrich. Acetone (99.9%), toluene (99.9%) and ethanol (90%) were obtained from Fisher Scientific. All chemicals and solvents were used as received without further purification.

### Synthesis of Cu-poor CZTS nanocrystals

All the CZTS NCs were prepared based on a modified heat-up protocol for CIGS NCs previously reported by Dilena *et al.*[44] The Cu-poor samples were achieved by tuning the precursor molar ratios of Cu:(Zn+Sn). Typically, a metal cationic precursor solution was prepared by degassing a mixture containing $CuCl_2.2H_2O$ (1.0 mmol Cu), $ZnCl_2$ (0.8 mmol Zn) and $SnCl_2$ (0.5 mmol Sn), 8 mL ODE and 8 mL OM in a 50 mL three-necked flask sealed with rubber septa, at 130 °C under vacuum for 30 min, followed by cooling to room temperature (RT) under Ar atmosphere. The S anionic precursor solution as-prepared by dissolving elemental S (5.2 mmol) in 2 mL OM and 2 mL ODE at 130 °C and followed by cooling to RT was added into the cationic precursor solution and the system was degassed at RT for additional 30 min. The as-obtained dispersion was then put under Ar atmosphere and heated up to 220 °C, and the reaction was kept at this temperature for 30 min. The heating mantle was then removed and the reaction vessel was allowed to cool to RT. The resulted dark brown solution was cleaned twice by ethanol followed by centrifugation at 4000 rpm for 5 min , and finally was dispersed in toluene (4 mL) for further characterizations. The precursor molar ratios of Cu:(Zn+Sn) was tuned in order to investigate its effect on the final composition of CZTS, and aliquots were collected during the heating up in order to monitor the formation mechanism of CZTS NCs. In the synthesis of bullet-like NCs CZTS, DT was introduced when we prepared the cation precursor. The gram-scale synthesis of CZTS NCs was performed by using the same procedure mentioned above except all of the precursors, solvent and ligand were scaled up to 10 fold and the flask was 1000 mL.

### Transmission electron microscopy (TEM) analysis

TEM and high-resolution TEM (HRTEM) measurements were performed on a JEM 2100F (Japan) microscope equipped with a field emission gun working at 200 kV accelerating voltage. The samples were prepared by drop-casting nanocrystal (NC) solutions on copper grids covered with an ultrathin amorphous carbon film, which were then placed in a high vacuum pumping station in order to let the solvent evaporate completely and preserve the NCs from oxidation. The energy dispersive X-ray spectroscopy (EDS) elemental maps of Cu, Zn, Sn and S were collected with high angle annular dark field scanning TEM (HAADF-STEM) mode on a Tecnai G2 F30 (FEI, Holland) microscope. For STEM-EDS elemental mapping the sample was prepared by drop-casting NC solutions onto carbon-coated gold grids.

### Powder X-ray diffraction (XRD)

The phase and crystallinity of the as-prepared samples were characterized by XRD on a Bruker D8 Advanced X-ray diffractometer with a Cu-Kα X-ray source under the operation conditions of 40 kV and 40 mA. The specimens were prepared in an Ar-filled glove box by drop casting the concentrated NC solution onto glass substrate followed by drying.

### ICP-AES analysis

Inductively Coupled Plasma Atomic Emission Spectroscopy (ICP-AES) was performed on Prodigy 7 spectrometer (LEEMAN LABS Ltd) for quantification of elemental composition of NC samples. The samples were decomposed in aqua regia ($HCl/HNO_3$ equal to v:v=3:1) overnight prior to the measurements.

### UV-Vis-NIR spectroscopy

UV-Vis-NIR extinction spectra on the as-achieved CZTS NCs were performed on a UV1601PC spectrophotometer (Shimadzu, Japan) at RT in the range of 300-2000 nm. The NPs dispersed in toluene were transferred in a cuvette and sealed, and taken out of the Ar-filled glove box for the optical spectra measurement.

### X-ray photoelectron spectroscopy (XPS)

The samples for XPS were prepared in the Ar-filled glove box by drop-casting NC solutions on a glass substrate, which was then transferred to the XPS set-up. Measurements were performed on a Thermo scientific 250 Xi spectrometer with a monochromatic Al Kα X-ray source (15 kV, 20 mA). The pressure in the analysis chamber was maintained below $9\times10^{-10}$ Torr for data acquisition. The binding energy (BE) scale was internally referenced to the C 1s peak (BE for C-C = 284.8 eV).

View Article Online
DOI: 10.1039/C7CE00223H




**Thermo gravimetric analysis (TGA)**

The measurement of mass changes and thermal effects between 25 °C to 600 °C has been carried out using Simultaneous Thermal Analyzer (STA 449 F3 Jupiter). Powder sample of CZTS NC were used for analysis TG-DSC under Ar atmosphere.

## Results and discussion

**Synthesis of pseudospherical and rice-like Cu-poor CZTS NCs**

We noticed that the final fraction of each element in the resulting CZTS NCs didn't match the molar ratios designed in the precursor. The Cu is rich and content of Zn is very low, which is due to the low reactivity of $Zn^{2+}$ ions (relative to Cu and Sn) with S species.[17] Indeed, in a designed synthesis with stoichiometric precursor, that is, by fixing starting Cu:Zn:Sn:S molar ratio as 2:1:1:4, we observed that the atomic percentages of the final CZTS NCs is 27.6, 4.0, 15.8 and 52.6% (found by ICP analysis), respectively, indicating a composition of $Cu_{2.1}Zn_{0.3}Sn_{1.2}S_4$ (see the details in Fig. S1 of the Electronic Supporting Information (ESI)). Consequently, we increased the starting $Zn^{2+}$ fraction and decreased the $Cu^{2+}$ amount in the precursors in order to obtain Cu-poor CZTS NCs. The TEM/HRTEM images, XRD patterns and optical spectra of the representative samples are displayed in Fig. 1 and more details are reported in Fig. S2-S4 of the ESI. As depicted in Fig. 1a-c and ESI Fig. S3, all of the resulting CZTS NCs are uniform in size. The majority of NPs were in pseudospherical shape when the precursor Cu:(Zn+Sn) ratio was in the range from 1:1.3 to 0.8:1.3 (Fig. 1a,b). However, some NPs were rice-like in case of starting Cu:(Zn+Sn) ratio below 0.6:1.3 (Fig. 1c). The analyses of XRD patterns ambiguously identified that kesterite hexagonal phase (JCPDS: 00-026-0575) of CZTS was formed both in the Cu-rich CZTS NCs (Fig. S1 of the ESI) and in the Cu-poor ones in case of starting Cu:(Zn+Sn) ratio higher than 0.6:1.3, without other phases or side-products formed in the resulting sample (Fig. 1g and Fig. S2e of the ESI). The XRD patterns with peaks at 28.5°, 47.3°, and 56.1° could be indexed with the planes (112) (220) and (312) in kesterite phase of CZTS NCs. The HRTEM analyses (Fig. 1d-f) on the typical single NPs of the above three samples are in good accordance with the XRD identification. However, as the Cu-poor increased, secondary phase of orthorhombic SnS (JCPDS: 00-014-0620) was also identified from XRD analysis besides kesterite phase of CZTS (see the details in Fig S2e-f of the ESI), which indicated that the direct reaction between $Sn^{2+}$ with $S^{2-}$ is not ignored in the presence of much more excess Sn precursor. We also noticed that in this case the resulting sample contained some pyramid-like NCs, which were further identified as orthorhombic phase of SnS NCs by HRTEM analysis (Fig. S4 of the ESI).

Based on the RT UV-Vis-NIR absorption spectra (Fig. 1h), the direct $E_g$ of the representative three Cu-poor CZTS samples determined *via* plotting $(\alpha hv)^2$ as a function of the photon energy (*hv)* (α=absorption coefficient, *h*=Plank's constant, *v*=frequency), were 1.53, 1.5 and 1.42 eV, respectively (Fig. S2h of the ESI).[45] These results are consistent with the previously-reported $E_g$ values of CZTS NCs obtained by various approaches.[13, 45, 46]

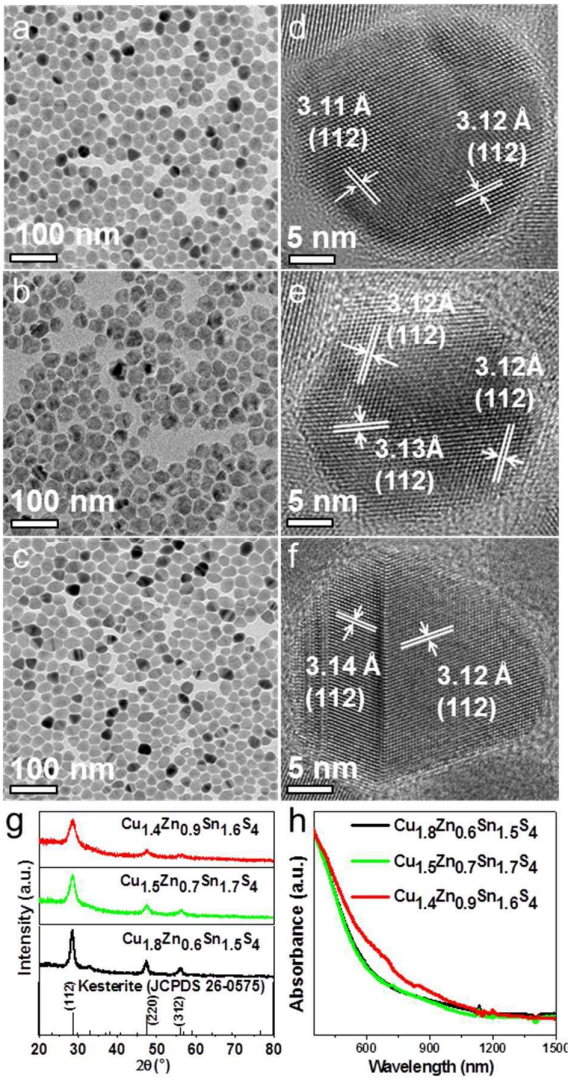


**Fig. 1** (a-f) Morphological characterization of the representative Cu-poor CZTS samples and corresponding single nanocrystals: TEM (a-c) and HRTEM (d-f) images of Cu-poor CZTS NCs with compositions of $Cu_{1.8}Zn_{0.6}Sn_{1.5}S_4$ (Cu:(Zn+Sn)=14%) (a,d), $Cu_{1.5}Zn_{0.7}Sn_{1.7}S_4$ (Cu:(Zn+Sn)=37.5%) (b,d) and $Cu_{1.4}Zn_{0.9}Sn_{1.6}S_4$ (Cu:(Zn+Sn)=44%) (c,f), respectively. The composition was found by ICP analyses. XRD patterns (g) and absorption spectra (h) of the corresponding Cu-poor CZTS NCs shown in a-c. The kesterite (JCPDS No. 00-026-0575) database is provided at the bottom of panel g.

**Synthesis of Cu-poor bullet-like CZTS NCs**

The reactivity of cation or anion precursors, reaction temperature and the ligand species were found to be important factors for the control of the crystallographic phase in synthesis of CZTS NCs.[17, 19, 33] It is interesting that by introduction of DT, we obtained bullet-like CZTS NCs, which evolved to wurtzite phase as DT amount increased (Fig. 2b-c and Fig. S5 in the ESI). We noticed that the diffraction peaks at 28.5°, 47.3°, and 56.1° could be assigned to either the planes (112) (220) and (312) of kesterite or the planes (002) (110) and (112) of wurtzite phase, respectively. However, the emerging

View Article Online
DOI: 10.1039/C7CE00223H




peaks at around 27.1°, 30.7° and 51.7° as DT increased to more than 2 mL are ambiguously indexed to the (100), (101) and (103) planes of wurtzite, respectively (Fig. 2g, green and red curves).[45, 47] The attribution of wurtzite phase is further evidenced by HRTEM analyses on single NCs (Fig. 2e-f). The crystal planes in some single NCs are not regular due to the defects. The phase evolution in our work is in agreement with what observed by Li et al.,[19] that is, the highly reactive small molecule $H_2S$ generated by reaction of elemental sulfur with OM yielded the formation of kesterite phase, however, the reaction in the presence of long alkane chain DT led to the formation of wurtzite phase. Furthermore, the DT functioned as not only S precursor but also capping ligand, which tailored the growth of nuclei and led to the formation of bullet-like NPs.

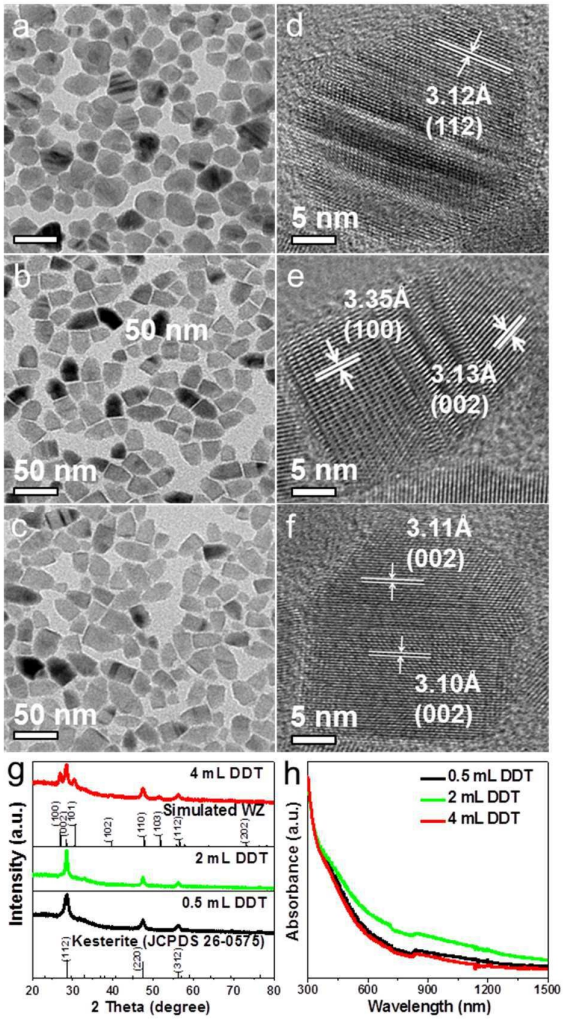


**Fig. 2** (a-c) TEM and (d-f) HRTEM images illustrating the bullet-like CZTS NCs obtained at 220 °C for 30 min in presence of different amounts of DT: 0.5 mL (a,d), 2 mL (b,e) and 4 mL (c,f). XRD patterns (g) and optical spectra (h) of the corresponding CZTS NCs shown in a-c.

**Growth mechanism of Cu-poor CZTS NCs**

In order to gain deep insight into the formation mechanism of the Cu-poor quaternary CZTS NCs, we collected the intermediated NCs by cleaning and precipitating various aliquots at different temperatures during the heat-up, and monitored their evolution of morphology, size, phase and optical spectra (Fig. 3 and ESI Fig. S6-S7 of the ESI). It is noteworthy that binary covellite phase (CuS) of NPs was already formed at RT (Fig. 3a, d, g), which evolved to bigger NPs by keeping overall the covellite phase with small amount of Zn (1% relative to Cu, found by ICP analyses) and Sn (8% relative to Cu) at 150 °C (Fig. 3b, e, g). The lattice fringes of the NC identified from HRTEM images exhibits interplanar distance of 1.87 Å, which is attributed to the (110) plane of covellite phase and is consistent with the XRD characterization (Fig. 3d-e). Quaternary kesterite CZTS NCs were formed when the temperature was raised up to 220 °C (Fig. 3c, f, g). Overall the average size in diameter of the aliquots increased with increasing reaction temperature, from approx. 4.0±0.5 nm at RT, to 13.5±2.5 nm at 150 °C and finally to 19.4±2.4 nm at 220 °C (Fig. S7 of the ESI). The conversion from binary NPs to quaternary CZTS could be also evidenced by evolution of optical spectra of the various aliquots (Fig. 3h), among which the NPs collected at temperature bellow 150 °C exhibited a well-defined NIR plasmon absorbance, a feature of binary NCs of copper chalchogenides.[48, 49] In comparison, the absorbance intensity of CuS collected at RT is weaker than that of NCs collected at 150 °C, which might be due to the surface scattering of the NCs with small dimensions at RT.[50] With increasing reaction temperature the NIR plasmon absorbance faded and finally vanished due to the progressive diffusion of cations ($Zn^{2+}$ and $Sn^{2+}$) into the as-formed covellite CuS NCs and to the formation of quaternary CZTS, during which the NCs grew progressively bigger. We need to point it out that the diffusion of foreign cations into CuS NCs could proceed even at 150 °C by keeping the reaction for longer time (e.g. 30 min), which also allowed the conversion from Zn-Sn-codoped CuS to quaternary CZTS NCs (Fig. S8a,g of the ESI), although the resulting NCs are not uniform in size compared with those achieved at higher temperatures (Fig. S8b-c of the ESI).

The conversion from binary copper sulfide nanoparticles (NPs) to ternary or quaternary ones was observed either in a direct preparation or in a post-chemical synthesis of CZTS NCs, which usually involved the partial cation exchange (CE) between $M^{x+}$ (M=In, Zn, etc.) and $Cu^+$ within $Cu_2S$ or $Cu_{2-x}S$ with composition close to $Cu_2S$ (e.g. $Cu_{1.94}S$).[51-53] Pateter et al. reported the transformation from $Cu_{2-x}S$ (close to $Cu_2S$) to CZTS *via* CE during the synthesis of CZTS NCs by using a hot injection of DT into the metal precursors at 150 °C followed by heating up to 250 °C for 60 min.[53] Stam et al. reported the $CuInS_2$ (CIS) synthesis by partial CE in $Cu_{2-x}S$ NCs.[54] This partial CE even worked in alloyed $Cu_{2-x}S_ySe_{1-y}$, which acted as seeds for the formation of Zn- and Sn-exchanged NPs.[55] $Cu_2S$ ($Cu_{2-x}S$ close to $Cu_2S$ as well) readily undergo CE due to the relatively mobile $Cu^+$ ions in a stable anionic framework of $S^{2-}$, which allowed for the substitution of $Cu^+$ with guest cations under the specified environment. However, the mechanism of the conversion from covellite CuS seeds formed at RT to quaternary CZTS NCs with increasing temperature is different with that previously reported. The crystals structure of covellite CuS is different with that of $Cu_2S$

View Article Online
DOI: 10.1039/C7CE00223H




due to the presence of S-S covalent bonds. In general, the CE on CuS or incorporation of CuS with foreign cations involve the rupture of S-S bonds and re-organization of anion framework, which requires appropriate electron donor such as ascorbic acid.[56] In the present work, OM and ODE might act as reducing agent to provide electrons particularly at high temperature,[57] which triggered the breaking S-S bonds and thus facilitated the incorporation of the as-formed CuS NCs by $Zn^{2+}$ and $Sn^{2+}$ ions.

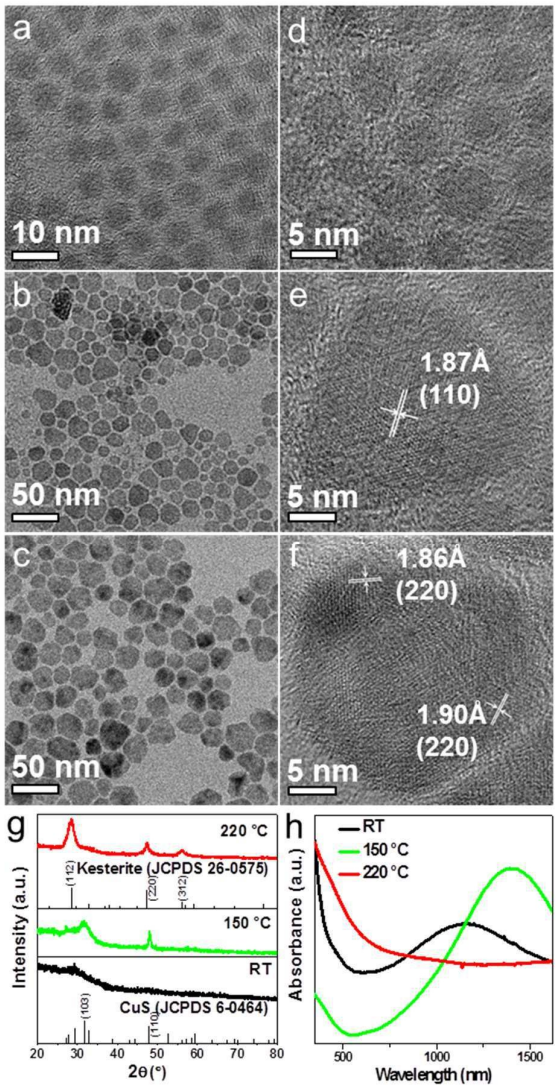


**Fig. 3** (a-f) TEM (a-c) and HRTEM (d-f) images of the aliquots collected at different reaction temperature during the heating up. XRD patterns (g) and optical spectra (h) of the corresponding samples shown in a-c.

A survey XPS spectrum of the representative Cu-poor CZTS NCs identifies the presence of the Cu 2p, Sn 3d, Zn 2p and S 2p (Fig. S9a of the ESI). Consider that the oxidation states of Cu and Sn in the as-reported CZTS are +1 and +4,[46] respectively, which are different with the corresponding valence states in their precursors ($CuCl_2.2H_2O$, $SnCl_2$), high resolution XPS was performed and four constituting elements of CZTS NCs was analyzed (Fig. 4). The peaks located at 931.3 eV and 951.3 eV with a split orbit of 20.0 eV matches well with the binding energies (BE) of Cu $2p_{3/2}$ and Cu $2p_{1/2}$, respectively, which unambiguously confirms the assignment of monovalent state of Cu ions ($Cu^+$) (Fig. 4a). We noted that the oxidation state of copper is solely $Cu^+$ since no any $Cu^{2+}$ satellites are observed from XPS. The Sn 3d core peaks split into $3d_{5/2}$ (485.7 eV) and $3d_{3/2}$ (494.3 eV), respectively, which could be assigned to the tetravalent state of tin ion ($Sn^{4+}$) (Fig. 4b). The XPS peaks of Zn 2p centred at 1020.1 eV (2p3/2) and 1043.2 eV (2p1/2), respectively, are in accordance with the valence value of $Zn^{2+}$. The spectrum of S 2p could be splitted into two peaks located at 161.3 eV (S $2p_{1/2}$) and 162.4 eV (S $2p_{3/2}$) (Fig. S9b of the ESI), respectively, which is consistent with mono-sulfide ($S^{2-}$). All these analyses of valence states are in agreement with the previously reported XPS results of the corresponding elements in CZTS compounds.[46]

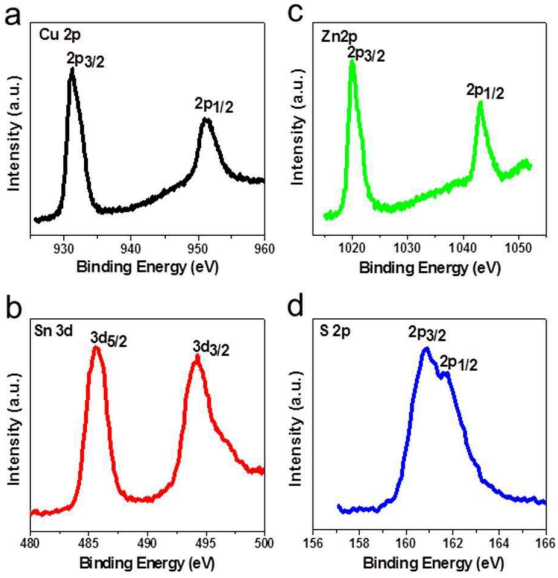


**Fig. 4** High resolution XPS of Cu 2p, Zn 2p Sn 3d, and S 2p from the Cu-poor CZTS NCs.

**Reproducible gram-scale synthesis**

The heat-up synthetic approach in our work can provide a desirable procedure for gram-scale synthesis of Cu-poor CZTS NCs with reproducible phase, composition, morphology and optical absorption spectrum. We confirmed the scalability in a 1000 mL flask by increasing 10-fold amounts of all chemicals, solvent and capping ligand relative to the typical synthesis previously described in the experimental section. That is, 40 mL of S precursor solution (S pre-dissolved in 20 mL of ODE and 20 mL of OM) was added in 160 mL metals dispersion with 80 mL of ODE and 80 mL of OM. The mixture was then degassed at RT for 30 min, followed by heating up to 220 °C under Ar flow and reacting for 30 min to produce the CZTS NCs. Fig. 5 and Fig. S10 of the ESI report the characterization results of the up-scaled synthesis, from which one can see kesterite phase of CZTS NCs with uniform size (16.8 ± 1.6 nm) was indeed achieved. The STEM-EDS elemental maps of a typical group of NCs confirmed

View Article Online
DOI: 10.1039/C7CE00223H


the homogeneity in composition since the Cu, Zn, Sn and S were evenly distributed inside the NCs, with a final average Cu:Zn:Sn:S molar ratio 1.8:0.7:1.5:4.0 (Fig. 5 and Fig. S10 of the ESI). The band gap energy calculated by plotting $(\alpha h\nu)^2$ versus $h\nu$ was 1.39 eV (Fig. S10c of the ESI). We noted that the synthesis yields of the Cu-poor CZTS NCs estimated based on the comparison of the total weight of the final compound and that of the starting precursors, where the ligand weight calculated from TGA analysis was subtracted, is only 48.47% due to the low reactivity of $Zn^{2+}$ with S species. All these results are in consistent with the characterization of small-scale synthesized sample (Fig. 1a,d,g-h) and all these features render our synthetic route able to easily reproduce Cu-poor CZTS NCs with uniform shape and size, homogenous composition and gram-scale product.

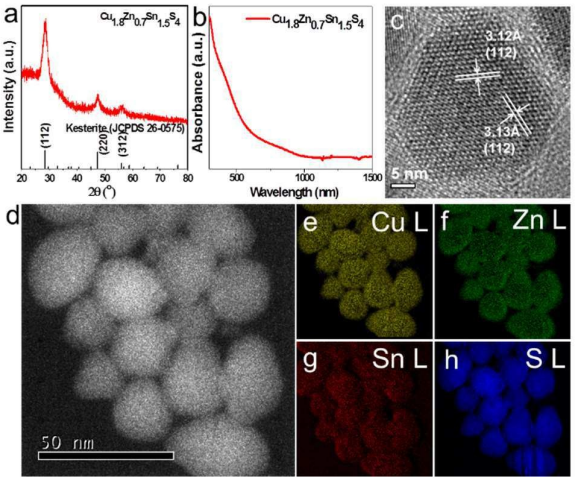


**Fig. 5** Characterization results of Cu-poor CZTS NCs obtained *via* large-scale synthesis: (a) XRD pattern, (b) optical spectrum, and (c) HRTEM image. (d) STEM-HAADF image of a group of Cu-poor CZTS NCs and (e-h) corresponding Cu, Zn, Sn and S EDS elemental maps.

## Conclusions

We have demonstrated a facile heat-up synthetic approach to prepare kesterite Cu-poor CZTS NCs with tunable composition and shape. This method involved the formation of binary CuS NPs at low temperature (e.g. RT), the Zn-Sn-codoped CuS as intermediate during the heating, and finally the quaternary CZTS NCs at high temperature due to the progressive incorporation of binary NPs by $Zn^{2+}$ and $Sn^{2+}$ cations. The introduction of DT led to the formation of bullet-like CZTS NCs with wurtzite phase instead of kesterite. We noticed that even the precursors of metal cations are $CuCl_2$ and $SnCl_2$, the oxidation states of Cu and Sn in the final CZTS products are +1 and +4, respectively. The proposed synthetic methodology provides a promising route for Cu-based NCs with the potential applications such as PVs due to the tunability and scalability of the reaction.

## Acknowledgements

This work was partially supported by NSFC (No. 51461135004), the China Postdoctoral Science Foundation for Priority Areas (No. 20130143130002), the Scientific Leadership Training Program of Hubei Province and the Scientific and Technical Innovation Project of Hubei Province (2013AEA005), the Fundamental Research Funds for the Central Universities (Wuhan University of Technology, WUT) (Grant No. 2016IVA095), and the Postdoctoral Science Foundation of WUT (Grant No. 408-32203). We also thank Dr. Xiaoqing Liu (Center of Materials Research and Testing, Wuhan University of technology) for help with HRTEM characterization.

## Notes and references

1 R. Tang, Z. Xie, S. Zhou, Y. Zhang, Z. Yuan, L. Zhang and L. Yin, *ACS Appl. Mater. Interfaces*, 2016, **8**, 22201-22212.
2 D. Tiwari, T. Koehler, X. Lin, R. Harniman, I. Griffiths, L. Wang, D. Cherns, R. Klenk and D. J. Fermin, *Chem. Mater.*, 2016, **28**, 4991-4997.
3 X. Liu, J. Huang, F. Zhou, F. Liu, K. Sun, C. Yan, J. A. Stride and X. Hao, *Chem. Mater.*, 2016, **28**, 3649-3658.
4 U. V. Ghorpade, M. P. Suryawanshi, S. W. Shin, C. W. Hong, I. Kim, J. H. Moon, J. H. Yun, J. H. Kim and S. S. Kolekar, *Phys. Chem. Chem. Phys.*, 2015, **17**, 19777-19788.
5 L. Arora, P. Gupta, N. Chhikara, O. P. Singh, N. Muhunthan, V. N. Singh, B. P. Singh, K. Jain and S. Chand, *Appl. Nanosci.*, 2015, **5**, 163-167.
6 M. Ibáñez, R. Zamani, A. LaLonde, D. Cadavid, W. Li, A. Shavel, J. Arbiol, J. R. Morante, S. Gorsse, G. J. Snyder and A. Cabot, *J. Am. Chem. Soc.*, 2012, **134**, 4060-4063.
7 M. Ibáñez, D. Cadavid, R. Zamani, N. García-Castelló, V. Izquierdo-Roca, W. Li, A. Fairbrother, J. D. Prades, A. Shavel, J. Arbiol, A. Pérez-Rodríguez, J. R. Morante and A. Cabot, *Chem. Mater.*, 2012, **24**, 562-570.
8 D. Chen, Y. Zhao, Y. Chen, B. Wang, Y. Wang, J. Zhou and Z. Liang, *ACS Appl. Mater. Interfaces*, 2015, **7**, 24403-24408.
9 Q. Guo, G. M. Ford, W.-C. Yang, B. C. Walker, E. A. Stach, H. W. Hillhouse and R. Agrawal, *J. Am. Chem. Soc.*, 2010, **132**, 17384-17386.
10 R. Zhang, S. M. Szczepaniak, N. J. Carter, C. A. Handwerker and R. Agrawal, *Chem. Mater.*, 2015, **27**, 2114-2120.
11 Q. Guo, H. W. Hillhouse and R. Agrawal, *J. Am. Chem. Soc.*, 2009, **131**, 11672-11673.
12 D. B. Mitzi, O. Gunawan, T. K. Todorov, K. Wang and S. Guha, *Sol. Energy Mater. Sol. Cells*, 2011, **95**, 1421-1436.
13 S. C. Riha, B. A. Parkinson and A. L. Prieto, *J. Am. Chem. Soc.*, 2009, **131**, 12054-12055.
14 H. Zhou, W.-C. Hsu, H.-S. Duan, B. Bob, W. Yang, T.-B. Song, C.-J. Hsu and Y. Yang, *Energy Environ. Sci.*, 2013, **6**, 2822-2838.
15 Y. B. K. Kumar, G. S. Babu, P. U. Bhaskar and V. S. Raja, *Phys. Status Solidi A*, 2009, **206**, 1525-1530.
16 M. Ibáñez, T. Berestok, O. Dobrozhan, A. LaLonde, V. Izquierdo-Roca, A. Shavel, A. Pérez-Rodríguez, G. J. Snyder and A. Cabot, *J. Nanopart. Res.*, 2016, **18**, 226-233.
17 Y. Zou, X. Su and J. Jiang, *J. Am. Chem. Soc.*, 2013, **135**, 18377-18384.
18 Y. Li, Q. Han, T. W. Kim and W. Shi, *Nanoscale*, 2014, **6**, 3777-3785.
19. Z. Li, A. L. K. Lui, K. H. Lam, L. Xi and Y. M. Lam, *Inorg. Chem.*, 2014, **53**, 10874-10880.
20 K. Yu and E. A. Carter, *Chem. Mater.*, 2016, **28**, 4415-4420.

View Article Online
DOI: 10.1039/C7CE00223H



21 S. Chen, X. G. Gong, A. Walsh and S.-H. Wei, *Appl. Phys. Lett.* , 2010, **96**, 021902-021904.
22 K. Tanaka, Y. Fukui, N. Moritake and H. Uchiki, *Sol. Energy Mater. Sol. Cells*, 2011, **95**, 838-842.
23 J. Fu, Q. Tian, Z. Zhou, D. Kou, Y. Meng, W. Zhou and S. Wu, *Chem. Mater.*, 2016, **28**, 5821-5828.
24 C. Jiang, Y.-T. Hsieh, H. Zhao, H. Zhou and Y. Yang, *J. Am. Chem. Soc.*, 2015, **137**, 11069-11075.
25 H. Xin, J. K. Katahara, I. L. Braly and H. W. Hillhouse, *Adv. Energy Mater.*, 2014, **4**, 1301823-1301827.
26 T. Schnabel, M. Löw and E. Ahlswede, *Sol. Energy Mater. Sol. Cells*, 2013, **117**, 324-328.
27 L. Wu, S.-Y. Chen, F.-J. Fan, T.-T. Zhuang, C.-M. Dai and S.-H. Yu, *J. Am. Chem. Soc.*, 2016, **138**, 5576-5584.
28 J. Zhong, Z. Xia, C. Zhang, B. Li, X. Liu, Y.-B. Cheng and J. Tang, *Chem. Mater.*, 2014, **26**, 3573-3578.
29 A. D. Collord and H. W. Hillhouse, *Chem. Mater.*, 2015, **27**, 1855-1862.
30 C. Jiang, W. Liu and D. V. Talapin, *Chem. Mater.*, 2014, **26**, 4038-4043.
31 J. van Embden, A. S. R. Chesman and J. J. Jasieniak, *Chem. Mater.*, 2015, **27**, 2246-2285.
32 A. S. R. Chesman, N. W. Duffy, S. Peacock, L. Waddington, N. A. S. Webster and J. J. Jasieniak, *RSC Adv.*, 2013, **3**, 1017-1020.
33 P. An, Z. Liang, X. Xu, X. Wang, H. Jin, N. Wang, J. Wang and F. Zhu, *RSC Adv.*, 2015, **5**, 6879-6885.
34 S. K. Saha, A. Guchhait and A. J. Pal, *Phys. Chem. Chem. Phys.*, 2012, **14**, 8090-8096.
35 H. Yang, L. A. Jauregui, G. Zhang, Y. P. Chen and Y. Wu, *Nano Lett.*, 2012, **12**, 540-545.
36 S. Singh, M. Brandon, P. Liu, F. Laffir, W. Redington and K. M. Ryan, *Chem. Mater.*, 2016, **28**, 5055-5062.
37 S. Singh, P. Liu, A. Singh, C. Coughlan, J. Wang, M. Lusi and K. M. Ryan, *Chem. Mater.*, 2015, **27**, 4742-4748.
38 S. Engberg, Z. Li, J. Y. Lek, Y. M. Lam and J. Schou, *RSC Adv.*, 2015, **5**, 96593-96600.
39 W. C. Liu, B. L. Guo, X. S. Wu, F. M. Zhang, C. L. Mak and K. H. Wong, *J. Mater. Chem. A*, 2013, **1**, 3182-3186.
40 B. D. Chernomordik, A. E. Beland, N. D. Trejo, A. A. Gunawan, D. D. Deng, K. A. Mkhoyan and E. S. Aydil, *J. Mater. Chem. A*, 2014, **2**, 10389-10395.
41 Y.-X. Wang, M. Wei, F.-J. Fan, T.-T. Zhuang, L. Wu, S.-H. Yu and C.-F. Zhu, *Chem. Mater.*, 2014, **26**, 5492-5498.
42 C. Steinhagen, M. G. Panthani, V. Akhavan, B. Goodfellow, B. Koo and B. A. Korgel, *J. Am. Chem. Soc.*, 2009, **131**, 12554-12555.
43 D. Aldakov, A. Lefrancois and P. Reiss, *J. Mater. Chem. C*, 2013, **1**, 3756-3776.
44 E. Dilena, Y. Xie, R. Brescia, M. Prato, L. Maserati, R. Krahne, A. Paolella, G. Bertoni, M. Povia, I. Moreels and L. Manna, *Chem. Mater.*, 2013, **25**, 3180-3187.
45 X. Lu, Z. Zhuang, Q. Peng and Y. Li, *Chem. Commun.*, 2011, **47**, 3141-3143.
46 M. Li, W.-H. Zhou, J. Guo, Y.-L. Zhou, Z.-L. Hou, J. Jiao, Z.-J. Zhou, Z.-L. Du and S.-X. Wu, *J. Phys. Chem. C*, 2012, **116**, 26507-26516.
47 C. Coughlan and K. M. Ryan, *Cryst. Eng. Comm.*, 2015, **17**, 6914-6922.
48 Y. Xie, L. Carbone, C. Nobile, V. Grillo, S. D'Agostino, F. Della Sala, C. Giannini, D. Altamura, C. Oelsner, C. Kryschi and P. D. Cozzoli, *ACS Nano*, 2013, **7**, 7352-7369.
49 Y. Xie, A. Riedinger, M. Prato, A. Casu, A. Genovese, P. Guardia, S. Sottini, C. Sangregorio, K. Miszta, S. Ghosh, T. Pellegrino and L. Manna, *J. Am. Chem. Soc.*, 2013, **135**, 17630-17637.
50 J. M. Luther, P. K. Jain, T. Ewers and A. P. Alivisatos, *Nat. Mater.*, 2011, **10**, 361-366.
51 L. Mu, F. Wang, B. Sadtler, R. A. Loomis and W. E. Buhro, *ACS Nano*, 2015, **9**, 7419-7428.
52 Q. A. Akkerman, A. Genovese, C. George, M. Prato, I. Moreels, A. Casu, S. Marras, A. Curcio, A. Scarpellini, T. Pellegrino, L. Manna and V. Lesnyak, *ACS Nano*, 2015, **9**, 521-531.
53 A. Pateter, W. Haas, B. Chernev, B. Kunert, R. Resel, F. Hofer, G. Trimmel and T. Rath, *Mater. Chem. Phys.*, 2015, **149–150**, 94-98.
54 W. van der Stam, A. C. Berends, F. T. Rabouw, T. Willhammar, X. Ke, J. D. Meeldijk, S. Bals and C. de Mello Donega, *Chem. Mater.*, 2015, **27**, 621-628.
55 V. Lesnyak, C. George, A. Genovese, M. Prato, A. Casu, S. Ayyappan, A. Scarpellini and L. Manna, *ACS Nano*, 2014, **8**, 8407-8418.
56 Y. Xie, G. Bertoni, A. Riedinger, A. Sathya, M. Prato, S. Marras, R. Tu, T. Pellegrino and L. Manna, *Chem. Mater.*, 2015, **27**, 7531-7537.
57 Z. Li, Y. Ji, R. Xie, S. Y. Grisham and X. Peng, *J. Am. Chem. Soc.*, 2011, **133**, 17248-17256.